SAND97-1969 C

To be presented at Surface Mount International '97, San Jose, CA, September 7-11, 1997 SAND--97-1969C

# Validating Theoretical Calculations of Thermomechanical Stress and Deformation Using the ATC4.1 Flip-Chip Test Vehicle†

RECEIVED
AUG 11 1997
OSTI

David W. Peterson, James N. Sweet, Steven N. Burchett
Sandia National Laboratories
Albuquerque, NM 87185-1082

CONF-970977--2

## ABSTRACT

Two closed form analytical solutions for tri-material thermomechanical stress and deformation, along with a one-quarter section finite element model (FEM), were validated using an in-situ CMOS piezoresistive stress measurement test chip that has been repatterned into a fine pitch area array flip-chip. A special printed circuit board substrate for the test chip was designed at Sandia and fabricated by the Hadco Corp. The flip-chip solder attach (FCA) and underfill was performed by a SEMATECH member company. The measured incremental stresses produced by the underfill are reported and discussed for two underfill materials used in this experiment. Detailed comparisons between theory and experiment are presented and discussed.

## KEY WORDS

flip chip, piezoresistor stress measurement, die stresses

## INTRODUCTION

The manufacturability and reliability of a flip-chip assembled package are strongly influenced by the mechanical stresses developed in the die-solder ball-substrate region. These stresses are produced by differential thermal contraction between substrate and die, and the stress distribution and magnitude can be significantly changed by the presence of an underfill material. It is highly desirable to model these stresses using analytical tools so that the susceptibility to mechanical failure during thermal cycling can be predicted for new geometries and combinations of materials without costly experimentation. However, the solder ball interface between an assembled flip-chip and substrate is particularly difficult to model precisely due to uncertain knowledge of both the elastic properties of the assembly constituents and the strain boundary conditions at material interfaces. One approach being investigated by the authors is use of a coarse resolution "global" model of the solder ball interface to supply appropriate strain boundary conditions to a high resolution "local" model. The "global" model is described in this paper. The FEM analysis accuracy is improved significantly by "calibration" using an *in situ* stress measurement technique, such as that described here and in previous work [1, 2] employing piezoresistor stress sensors. (A thorough treatment of Si piezoresistor stress measurement theory is contained in Ref. [3])

A flip-chip on laminate substrate, though somewhat simpler to model than a molded IC, is under a complex state of stress and strain due to large differences in thermal expansion between die and substrate. Interfacial stress is generally relieved through bending of the assembly and the magnitude of these stresses can be approximated with relatively simple "bimetallic strip" models. Hall [4] describes a spreadsheet technique that calculates in-plane stress at each interface of a multilayer structure. This method assumes a constant radius of curvature and does not account for end effects, but is useful for determining maximum states of compression or tension along the $z$ dimension of an assembly. Suhir [5] described a more sophisticated model that accounts for end effects and calculates the distribution of in- and out-of-plane compressive stress ($\sigma_{xx}$, $\sigma_{yy}$, and $\sigma_{zz}$), and interfacial shearing stress ($\tau_{xz}$, $\tau_{yz}$) components. There are numerous journal articles describing similar approaches, but we will use these two examples in the results section to compare with FEM calculations and experimental measurement data obtained from *in situ* stress sensors. The assembled flip chip has the unique quality that its surfaces can be easily measured for deflection, an important parameter that, combined with *in situ* stress data, can be very effective in validating analytical and FEM techniques.

## EXPERIMENTAL

### Test Vehicle Description

The ATC4.1 Assembly Test Chip, with a side dimension of 11.6 mm (0.456 in.) was repatterned for area array using a Cu-polyimide process. The eutectic solder bump array is square with 42 bumps per row (1764 total bumps) and a 0.0254 mm (0.010 in.) bump pitch. The chip contains 100 addressable stress sensing cells plus ring oscillators, resistive heaters, and diode thermometers described elsewhere [6]. All CMOS signals are brought out through perimeter balls, while inner balls are used for daisy chain and Kelvin ball resistance circuits. For the experiments discussed in this work, a special printed circuit board substrate was designed at Sandia and fabricated by the Hadco Corp. The flip-chip solder attach and underflow assembly was performed by a SEMATECH member company using a no-clean flux process. The layout for a single ATC4 die prior to redistribution and bumping is

---

† This work was supported by the United States Department of Energy under Contract DE-AC04-94AL85000. Sandia is a multiprogram laboratory operated by Sandia Corporation, a Lockheed Martin Company, for the United States Department of Energy.

DISTRIBUTION OF THIS DOCUMENT IS UNLIMITED

MASTER

## DISCLAIMER

**This report was prepared as an account of work sponsored by an agency of the United States Government. Neither the United States Government nor any agency thereof, nor any of their employees, make any warranty, express or implied, or assumes any legal liability or responsibility for the accuracy, completeness, or usefulness of any information, apparatus, product, or process disclosed, or represents that its use would not infringe privately owned rights. Reference herein to any specific commercial product, process, or service by trade name, trademark, manufacturer, or otherwise does not necessarily constitute or imply its endorsement, recommendation, or favoring by the United States Government or any agency thereof. The views and opinions of authors expressed herein do not necessarily state or reflect those of the United States Government or any agency thereof.**

## DISCLAIMER

Portions of this document may be illegible in electronic image products. Images are produced from the best available original document.

shown in **Figure 1**. A SEM micrograph of a bumped QUAD is shown in **Figure 2**.

**Figure 3** contains the repattern and bump process flow along with critical dimensions. An assembled part is shown in **Figure 4** and **Figure 5** shows relevant board and cross-section dimensions. **Figure 6** contains an SEM micrograph of an assembly cross-section.

**Table 1: Material Properties**

| | Si | Under-fill | Solder | FR-4 |
|---|---|---|---|---|
| Thickness (mm) | 0.69 | 0.051 | 0.51 | 0.762 |
| Length, width (mm) | 11.6 | 11.6 | | 45.7 |
| CTE ($10^{-6}$/°C) | 2.6 | 22 (A)<br>35 (B) | 25 | 14.7 |
| Elastic modulus (GPa) | 112.7 | 8.6 (A)<br>6.5 (B) | 43.1 | 15.5 |
| Poisson's ratio | 0.25 | 0.30 | 0.365 | 0.20 |

Material properties used in the analytical and FEM simulations are contained in **Table 1**. An additional solder property, yield stress = 34 MPa, was used in the FEM simulation prior to underfill. Some of the values used for these calculations were handbook properties because we did not have more accurate values available at the time.

**Electrical and Mechanical Measurements**

In order to relate changes in piezoresistor values due to changes in the state of die stress, it is necessary to develop a set of "reference" measurements at the wafer level. The die are not stress free at this point, but are considered to be under negligible stress compared to that seen during subsequent packaging operations. A manual wafer level probe is made, in which all 25 stress cells in each die (100 cells per QUAD) are sequentially interrogated under PC control through a common 4-point measurement bus using a precision current source and digital voltmeter. There are 900 floating point data per QUAD associated with these measurements that are entered into a reference data base. After redistribution and solder bumping, known good diced QUADs are identified and separated from the wafer using the results from these initial measurements.

A custom-made test fixture makes electrical connection to the three rows of perimeter pads on the FR-4 substrate using pogo pins. Signals are routed to a 144 I/O general purpose PC controlled test system via an interface board. The test system instruments are functionally equivalent to those used at the wafer level probe and provide similar short and long term accuracy. The assembled ATC4.1 QUADs contain more test structures than available at the wafer level–4-point solder ball resistance structures and daisy chains. Measurements are made on these structures along with stress cell resistance and diode measurements at defined test intervals during the course of an experiment, and are entered into a data base. Processing and analysis of these data are described in the Experimental Stress Analysis section. Test intervals for the work described here were before and after underfill.

Deflection of die and substrate were measured along the *x*-axis and *y*-axis using a Mahr S8P profilometer with a Focodyn laser stylus. A machined fixture was used to ensure proper alignment of the part during each of the four measurements. The tool was set to measure maximum deflection over a 6.35 mm (0.250 in.) path straddling the center of the 11.6 mm QUAD die. Measurements were made before and after underfill.

**2D Theoretical Stress Analysis**

There are a number of closed form analytical solutions to the tri-material die-on-substrate problem based on generalizations of the classical "bimetallic strip" problem. These solutions assume no external forces act on the structure and the sum of all forces and moments must be zero. The Hall [4] theory of stress in *n* layers is based on uniform layers in an axisymmetric disc ($\sigma_{xx} = \sigma_{yy}$) of infinite dimensions in the plane, where the thickness is much less than the in-plane dimensions. This solution does not take into account edge effects and assumes constant radius of curvature throughout the structure. Displacements are calculated at each material interface. Strain is assumed to vary linearly from one interface to the next within a layer as a function of the coordinate normal to the surface and is continuous across material boundaries. Within a given layer, stress is also assumed to vary linearly as a function of *z*, but is generally discontinuous between layers. The theory is implemented in a convenient spreadsheet formulation.

**Figure 7** shows a calculation of the vertical or z variation of the in-plane stress along the *y*-axis at the interface of each layer calculated using the Hall theory together with parameters from **Table 1** and thickness dimensions from **Figure 5**. It is based on stresses developed during cooldown from a stress free temperature of 160 °C to 20 °C ($\Delta T = 140$ °C). The solder ball underfill region is represented as a uniform homogeneous layer with the parameters of underfill, as given in **Table 1**. The spreadsheet also calculates radius of curvature of the assembly and assumes that it is constant throughout the plane. The Hall theory predicts slightly higher compressive stress and deflection for the underfill B material, which has lower elastic modulus, but considerably higher CTE.

Suhir [7] has presented a tri-material stress analysis model applicable to both face-up and flip-chip die attach methods and assumes rectangular geometry unbounded along one axis in the plane. The model is generally simplified to a bi-material solution for the case when the thickness and/or elastic modulus of the interstitial layer (in this case the solder ball array and underfill) are small. For this work we were specifically interested in differentiating between underfill materials so the "full" Suhir model was employed.

We included improvements to the model's estimation of the out-of-plane shear stress distribution ($\tau_{xz}$) and peel stress ($\sigma_{zz}$) magnitude [5]. The calculations shown in **Figure 8** are based on data in **Table 1** and $\Delta T$ = 140 °C. In this figure, the half width of the QUAD has been normalized, so that $y$ = 0 represents the QUAD center and $y$ = $L/2$ is the edge coordinate, or furthest distance from the neutral point along the $y$-axis. The model also calculates the radius of curvature distribution along the $y$-axis. These local radii are relatively constant in the center region of the die, correlating well in magnitude with the Hall calculation (both predict ρ=0.72 m at the center), and increase toward infinity approaching the die edge. Suhir theory also predicts slightly higher in-plane compressive stress, $\sigma_{yy}$, and smaller radius of curvature for the underfill B case.

**3D Theoretical Stress Analysis**

A 3D finite element model (FEM) was applied to predict the stress, strain, and deformation response of the ATC4.1 test vehicle due to 1) cool down to room temperature from the soldering temperature prior to underfill, and 2) due to cool down to room temperature from the cure temperature following underfill. The finite element idealization, shown in **Figure 9**, utilizes two planes of symmetry resulting in one quarter of the package being simulated using a high resolution 200,000 element model. This includes 441 solder interconnects-modeled using three eight-node brick elements per solder ball.

The solder was assumed to respond as an isotropic temperature dependent elastic/plastic material with power law hardening. This model neglects the time dependent (creep) and microstructural dependent response known to occur in eutectic SnPb solder. The underfill was assumed to respond as an isotropic temperature dependent linear elastic material which neglects time dependent effects known to occur in polymers. The Si die was assumed to respond as an isotropic linear elastic material and the FR-4 substrate was assumed to respond as a temperature dependent, isotropic, linear elastic material.

In the first computation, it was assumed that the assembly prior to underfill was stress free at 180 °C and subsequently cooled to 20 °C. In the second computation, the assembly after underfill (UF A) was assumed to be stress free at 160 °C and the temperature was uniformly lowered to 20 °C. The thermomechanical response was computed as a function of temperature using the Sandia proprietary finite element code JAS3D and properties for underfill A in **Table 1**.

**Experimental Stress Analysis**

The subject of deriving stress data from experimental ATC04 stress measurements has been discussed extensively in Sweet et. al [8]. Here we provide some summary information to specify the data analysis process. In each stress sensor cell, there are 4 $n$-type and 4 $p$-type implanted resistors. They are numbered 1-4 and oriented at; 0, 45, 90, and 135°, respectively, with respect to the chip bottom edge, as shown in **Figure 10**. These resistors have nominal values in the range 8-10 kΩ, and stress induced changes typically are in the range 1-10 Ω, or about 0.01-0.1%. If the resistors are measured at some initial state (0) and again at some final state (f) after an intervening manufacturing or environmental process step, then the change in certain stress tensor components at the cell site can be derived from the resistor shifts, $\Delta R_i = R_{if} - R_{i0}$, where the index $i$ runs over the resistors in the cell.

It can be shown that all stress data depend on the $\Delta R$ values for a given resistor type only through the sum ($S$) or difference ($D$) of the relative resistor shifts of two resistors oriented 90° apart. These quantities, designated $\delta R_{ij}^{S,D}$, where $i$ and $j$ are 1 and 3 (0°, 90°) or 2 and 4 (45°, 135°) and $S$, $D$, refer to + and –, respectively, are given by,

$$\delta R_{ij}^{S,D} = \left( \frac{\Delta R_i}{R_{i0}} \pm \frac{\Delta R_j}{R_{j0}} \right). \tag{1}$$

In the case of $\delta R^D$, any shift in resistance values produced by a temperature shift $\Delta T$ in the ambient temperature between initial and final measurements cancels out. Thus stresses which depend only on a $\delta R^D$ value are intrinsically temperature compensated in that they do not require a correction for the temperature shift. In the case of stresses which depend on $\delta R^S$ values, a correction term, $2\alpha\Delta T$ is required, where $\alpha$ is the relative temperature coefficient of resistivity for the given resistor type, the fractional change in resistance per unit temperature change at constant external stress.

The quantities which may be derived from $\delta R^D$ measurements are the in-plane shearing stress, $\tau_{xy}$, and the difference of in-plane compressive stresses, $\sigma_{xx} - \sigma_{yy}$. These quantities are given by,

$$\tau_{xy} = \frac{\delta R_{24}^D}{2\pi_D}, \tag{2}$$

and,

$$\sigma_{xx} - \sigma_{yy} = \frac{\delta R_{13}^D}{\pi_{44}}. \tag{3}$$

The quantity $\pi_D$ in Eq.(2) is given by $\pi_D = \pi_{11} - \pi_{12}$, where $\pi_{11}$, $\pi_{12}$, and $\pi_{44}$ are the fundamental coupling constants or "pi" coefficients which relate stress changes to resistance shifts. $\pi_D$ has a large magnitude only for the $n$-type resistors, so the diagonal or 2-4 $n$-type resistor data are used to derive $\tau_{xy}$. In the case of $\sigma_{xx} - \sigma_{yy}$, $\pi_{44}$ for the $p$-type resistors has about five times the magnitude of the $n$-type $\pi_{44}$, so we use $p$-type data to derive the in-plane compressive stress difference from Eq.(3).

One other general relation which may be found for the stress tensor components is given by,

$$\sigma_{xx} + (\pi_{12}/\pi_S)\sigma_{zz} = \frac{\delta R_{24}^S - 2\alpha\Delta T}{2\pi^S} + \frac{\delta R_{13}^D}{2\pi_{44}}, \tag{4}$$

where $\pi_S = \pi_{11} + \pi_{12}$. Using the $\pi$ coefficients in Ref. [8], the quantity $\pi_{12}/\pi_s \approx -1.2$. In the case of a flip-chip attachment to a substrate, the magnitude of $\sigma_{zz}$ is very small relative to that of $\sigma_{xx}$ at all sensor locations and hence we shall just report data derived from the right hand side of Eq.(4) as $\sigma_{xx}$. Eq.(4) is equivalent to Eq.(7) in [8], but the latter equation has an error in the last term on the right where a factor of 2 in the denominator was omitted.

One final point which can be made is that the quantities $\delta R_{24}{}^S$ and $\delta R_{13}{}^S$ are theoretically equal, so a better experimental value for the first term on the RHS of Eq.(4) can be found by using the average value of these quantities to derive $\sigma_{xx}$. The expression used to find $\sigma_{xx}$ is given by,

$$\sigma_{xx} = \frac{\left(\delta R^S_{24n} + \delta R^S_{13n}\right)/2 - 2\alpha_n \Delta T}{2\pi^S_n} + \frac{\delta R^D_{13p}}{2\pi_{44p}}. \qquad (5)$$

In some cases, we are interested in looking at $\sigma_{yy}$ in addition to $\sigma_{xx}$. $\sigma_{yy}$ can be found by subtracting Eq. (3) from Eq.(5), resulting in the expression,

$$\sigma_{yy} = \frac{\left(\delta R^S_{24n} + \delta R^S_{13n}\right)/2 - 2\alpha_n \Delta T}{2\pi^S_n} - \frac{\delta R^D_{13p}}{2\pi_{44p}} \qquad (6)$$

**Table 2: $\pi$ and Temperature Coefficients**

| Coefficient | $n$-type | $p$-type |
|---|---|---|
| $\pi_{11}$ ($10^{-5}$/MPa) | -26.7 | |
| $\pi_{12}$ ($10^{-5}$/MPa) | 14.2 | |
| $\pi_S$ ($10^{-5}$/MPa) | -12.5 | |
| $\pi_{44}$ ($10^{-5}$/MPa) | -16.1 | 72.2 |
| $\alpha$ (°C$^{-1}$) | 0.001473 | 0.001147 |
| $\Delta T/\Delta Vbe$ (°C/V) | 557.2 | |

The $\pi$ coefficient values and other constants used in the data reduction are given in **Table 2**. These values were determined from a recent reanalysis of calibration data and are slightly different from the values reported in [8]. The $p$-type $\pi_{11}$, $\pi_{12}$, and $\pi_S$ values are very small in magnitude and could not be determined accurately. They are not used in any of the calculations reported in this paper.

## RESULTS

### Prior to Underfill

For the measurement of initial or as-assembled stresses, the initial condition was taken at the wafer level, prior to redistribution and bump processing. The final state was the measurement on the parts after flip-chip assembly to the FR-4 substrates. As discussed above, the differential thermal contraction between die and substrate after cooling from the solder reflow temperature to room temperature produces bending of the assembly with the consequent development of stresses in the die, substrate, and solder attachments. Since the substrate has a larger coefficient of thermal expansion than the Si die, the substrate shrinks more than the die, thus producing a convex or upward bending of the die center, with the bottom or active surface of the die in compression and the top or back surface in tension. We might expect that the outer solder bumps will take up some of the strain energy, with a consequent increase in bending radius along a path from the die center to the perimeter.

This effect was observed for a typical part in the measured compressive stress distribution for $\sigma_{yy}$ shown in **Figure 11.** In this plot, from our data analysis software, the rows and columns are on an equally spaced grid and hence the plot somewhat distorts the spatial variation of the stress. The distribution shows a decrease in the magnitude of $\sigma_{yy}$ as $y \rightarrow \pm L/2$, where $L$ = chip width. The distribution in measured $\sigma_{xx}$ or $\sigma_{yy}$ stress values across the chip surface is typically relatively "noisy" or variable from cell to cell, as seen in this figure, compared with similar measurements made on molded parts. The FEM data suggest that this is due to stress concentrations or non-uniformities at the die surface in the vicinity of each solder ball. This is illustrated in **Figure 12** for the case of $\sigma_{yy}$, where the in-plane compressive stress peaks slightly on the side of each solder ball facing the center and dips slightly on the other side. Similar stress concentrations at the die surface in the vicinity of the solder balls are evident in plots of the other components of the stress tensor.

The assembled part under study has nominal square symmetry. This symmetry condition implies that the variation of a compressive stress tensor component along any diagonal path from the chip center to a corner should be identical. Hence it is useful to examine the variation of $\sigma_{yy}$ along a chip half diagonal. A plot of $\sigma_{yy}$ data measured at seven stress sensor locations along a QUAD half diagonal and averaged across 27 parts is shown in **Figure 13.** Although there is a clear trend for the stress magnitude to decrease as the diagonal position moves from the chip center to a corner, as expected from basic principles, there is a curious "S" curve apparent in the plotted data. Overlaying the FEM calculations for the same locations suggests that this shape is real and predictable at least through the use of the FEM method, though not intuitive nor predictable using analytical models. (Hall and Suhir methods calculate stresses only on a major axis.)

An experimental quantity determined more precisely (temperature is intrinsically compensated) is the in-plane compressive stress difference function, $\sigma_{xx} - \sigma_{yy}$. By symmetry, we expect this quantity to be small at the chip center and along diagonal paths. The maximum variation is expected to be along the chip edge paths, $x = \pm L/2$ and $y = \pm L/2$, where due to square symmetry, variations should be the same along symmetrical paths. A plot of $\sigma_{xx} - \sigma_{yy}$ for one

of the four vertical paths through the outer vertical sensor columns (cells 18–25) averaged across 27 parts prior to underfill, is shown in **Figure 14**. The SD bars on the measured data do not so much represent the randomness of data at each point as they show the random variation in the overall stress distribution curves for the 27 parts. The predicted stress distribution based on FEM calculations is shown as unfilled circles in **Figure 14**. The large difference between experiment and theory is thought to be due to non-symmetric bending of the assembly caused by anisotropy in the elastic properties of the substrate. Measurements of substrate and die deflections with a non-contact laser profilometer before and after underfill confirmed that the assembled parts were bent more along the y-axis resulting in a higher $\sigma_{yy}$ stress component. These data are shown in **Figure 15**.

### After Underfill

After underfill, the in-plane compressive stress components become larger in magnitude and much more uniform over the chip surface, indicating that the state of chip bending is also more uniform. It is interesting to examine the changes in stress tensor components which occur between the assembly and underfill states because the predictions of these changes is a sensitive test for a finite element model analysis. The change in the in-plane compressive stress difference function, $\Delta(\sigma_{xx} - \sigma_{yy})$ is especially interesting because it has a significant variation over the die surface.

A 3D bar distribution plot of this measured stress function is shown for a single part in **Figure 16**. The function peaks at a value ≈ 25 MPa along the vertical die edges approximately half way between the QUAD centerline and the top or bottom QUAD $y$ coordinates. In the center it has a minimum with a value ≈ 9 MPa. The detailed spatial variation in this measured stress function provides an especially sensitive test or point of comparison for a finite element model. An examination of the in-plane compressive stress difference function with wafer level as the initial state and post-underfill as the final state shows that $\sigma_{xx} - \sigma_{yy} \approx 15$ MPa at the die center. Since both $\sigma_{xx}$ and $\sigma_{yy}$ are compressive in nature, this result indicates that there is more bending (smaller radius of curvature) in the $y$ direction than the $x$ direction. This was also true prior to underfill, but the difference then was only ≈ 3 MPa.

The FEM analysis reveals a reversal in the out-of-plane compressive stress, $\sigma_{zz}$, toward the QUAD corner. This component is expected to be very small except approaching the die edges where it should increase almost exponentially in the tensile direction. Thus the term "peel" stress is often applied to this component. The FEM calculation does predict ~35 MPa (tensile) at the edge adjacent to the substrate for the underfill A case at room temperature, but shows it becoming ~-28 MPa (compressive) at the corners. This can be seen in **Figure 17**.

### *Comparison of Experimental to Theoretical Calculations*

A useful stress component trajectory that can facilitate comparison between analytical, FEM, and experimental data is the in-plane compressive stress, $\sigma_{yy}$, along a centerline axis. We choose a path parallel to the $y$-axis but slightly offset from the centerline to coincide with the **Figure 1** stress sensor locations of cells 1-8. Measurement data and calculations are collected in **Figure 18** for comparison with experimental measurements on assembled parts both before and after underfill A. There are no comparisons made to analytical calculations for the prior to underfill case, as these models do not handle inhomogeneous properties in an interface region containing only solder balls, and also because the assumption of constant radius of curvature along the $z$-axis at each $x$-$y$ location is no longer valid. The latter can be seen graphically in **Figure 19**, where prior to underfill **(a)** the substrate and die have visibly different curvatures along points in the plane, and after underfill **(b)** the die and substrate follow the same bending radius except at the extreme edge of the QUAD. From **Figure 18** we see that the FEM calculations prior to underfill predict a linear decrease in compressive stress from the QUAD center to the edge, implying a constant *change* in the radius of curvature along this path. The corresponding experimental data correlate well with this trend except toward the QUAD center, where the stresses "flatten" out.

After underfill, both Suhir and Hall predict maximum $\sigma_{yy}$ stress magnitudes in close agreement with measured stresses that were averaged over 27 parts. The FEM calculations are also in good agreement and include the effects of localized stress gradients in the vicinity of the solder balls, as discussed earlier.

## DISCUSSION

The work discussed above demonstrates that many aspects of the measured die surface stresses in an underfilled flip-chip assembly can be successfully predicted with analytical tools along paths in and out of the plane and on major axes. The trends and magnitudes predicted using the Suhir theory, in particular, closely match experimental data gathered over many assemblies. This is in large part due to the square symmetry of the assembly which accommodates a 2D model containing one semi-infinite axis. On the other hand, the analytical methods do not provide insight into the state of thermomechanical stress prior to underfill, nor can they predict "second" order effects in a complex assembly after underfill, such as the reversal in peel stress at the die corners observed in **Figure 17**. The FEM technique provides this additional fidelity when a solder ball array macro model is used in place of a homogeneous model that takes on the average of the underfill and solder ball properties. In the data presented, this fidelity included detailed variations in stress caused by the mismatch in material properties between the solder, underfill, substrate and die. The prediction of stress prior to underfill, illustrated for the case of the in-plane compressive component in **Figure 18**, appears to correctly reflect the behavior of a complex flip chip

assembly except near the die center, based on correlation with experimental data. Plasticity and creep occur simultaneously during cool down from reflow temperature and we clearly need a better constitutive model and possibly more elements per solder ball to accurately predict this behavior, and this is the subject of continuing work.

The agreement between FEM and Suhir theory shown in **Figure 18** suggests that, for calculation of die stresses after underfill, it is reasonable to represent the underfill-solder ball region as a homogeneous layer with properties of the underfill. The assembly appears to be in a state of near uniform biaxial bending and is thus suitable for stress analysis with simplified analytical models.

The measurements of the in-plane compressive stress difference function, $\sigma_{xx} - \sigma_{yy}$, **Figures 14** and **16**, show that the FR-4 board CTE and/or elastic modulus are anisotropic. The die deflection data in **Figure 15** show a variation that is consistent with the stress difference data. This anisotropy was not built into the FEM model used for the analysis in this paper, but will be included in future model updates. Our result demonstrates how an experimental measurement of stress can be used to aid the development of more refined and accurate analysis techniques and to validate properties data used in the models.

## CONCLUSIONS

We have demonstrated that a high resolution FEM technique that incorporates a macro model of the solder ball array when applied to a flip chip assembly can provide unique insight into localized stress non-uniformities and stress reversals previously unpredicted. The ATC4.1 piezoresistive test chip used to validate these calculations was able to capture a good portion of this detail in what was previously considered measurement error or noise. The FEM technique developed as part of this work will be improved to better describe the stress-strain behavior prior to underfill, which will presumably improve its prediction of boundary conditions at each solder ball after underfill. Future work will attempt to couple a very high resolution solder ball model at a high stress location to the macro model and focus on fatigue life prediction.

The analytical techniques correlated well with both measurement data and FEM calculations along major axes and were sensitive to differences in underfill properties, though it was necessary to approximate or ignore the contribution of the solder ball array to the underfill region. The Suhir theory was more useful for the tri-material application studied, as it included edge effects and provided stress distributions in the plane. However, the Hall theory can provide excellent insight into bending and peak in-plane stress in assemblies with more than three layers. Both methods lend themselves to Monte Carlo simulation and sensitivity analysis.

## ACKNOWLEDGMENTS

The authors wish to thank the SEMATECH Liquid Encapsulant Enhancement (LEE) PTAB members – IBM, Lucent Technologies, National Semiconductor Corporation, Hewlett-Packard, and in particular, Emie Sorongon, the LEE PTAB project leader – for their ongoing and extensive support of this work. We also thank Robert Mitchell for measurement support, Simone Smith for SEM work, and Gary Peterson for assistance in board procurement and process development.

## REFERENCES

[1] J. N. Sweet, D. W. Peterson, J. A. Emerson, S. N. Burchett, "Experimental Measurements and Finite Element Calculations for Liquid Encapsulated ATC04 Assembly Test Chips," in *Proc. 1995 ASME Int. Mech. Engr. Congress, Applications of Experimental Mechanics to Electronic Packaging,* Vol. EPP-13, pp. 61-71.

[2] J. N. Sweet, D. W. Peterson, J. A. Emerson, R. T. Mitchell, "Liquid Encapsulant Stress Variations as Measured with the ATC04 Assembly Test Chip," *Proc. 45th Elec. Comp. & Tech. Conf.*, IEEE, 1995, pp. 294-300.

[3] For a review of the literature up to 1992 and a discussion of the technique, see: J. N. Sweet, "Die Stress Measurement Using Piezoresistive Stress Sensors," in J. H. Lau, editor, Thermal Stress and Strain in Microelectronics Packaging, Van Nostrand Reinhold, NY, 1993, pp. 221-271.

[4] P. M. Hall, "Thermal Expansivity and Thermal Stress in Multilayered Structures," in J. H. Lau, editor, Thermal Stress and Strain in Microelectronics Packaging, Van Nostrand Reinhold, NY, 1993, pp. 78-94.

[5] V. Mishkevich, E. Suhir, "Simplified Engineering Approach for the Evaluation of Thermally Induced Stresses in Bi-Material Microelectronic Structures," in E. Suhir, editor, Structural Analysis in Microelectronics and Fiber Optics," ASME Press, 1993, pp. 127-133.

[6] J. N. Sweet, D. W. Peterson, M. R. Tuck, and J. M. Greene, *Assembly Test Chip Ver. 04 (ATC04) Description and User's Guide*, Sandia National Laboratories Report, SAND93-1901.

[7] E. Suhir, "Die Attachment Design and Its Influence on Thermal Stresses," in *Proc. 37th Elec. Comp. Conf.*, IEEE, 1987, pp. 508-517.

[8] J. N. Sweet, D. W. Peterson, J. A. Emerson, S. N. Burchett, "Experimental Measurements and Finite Element Calculations for Liquid Encapsulated ATC04 Assembly Test Chips," in *Proc. 1995 ASME Int. Mech. Engr. Congress, Applications of Experimental Mechanics to Electronic Packaging,* Vol. EPP-13, pp. 61-71.

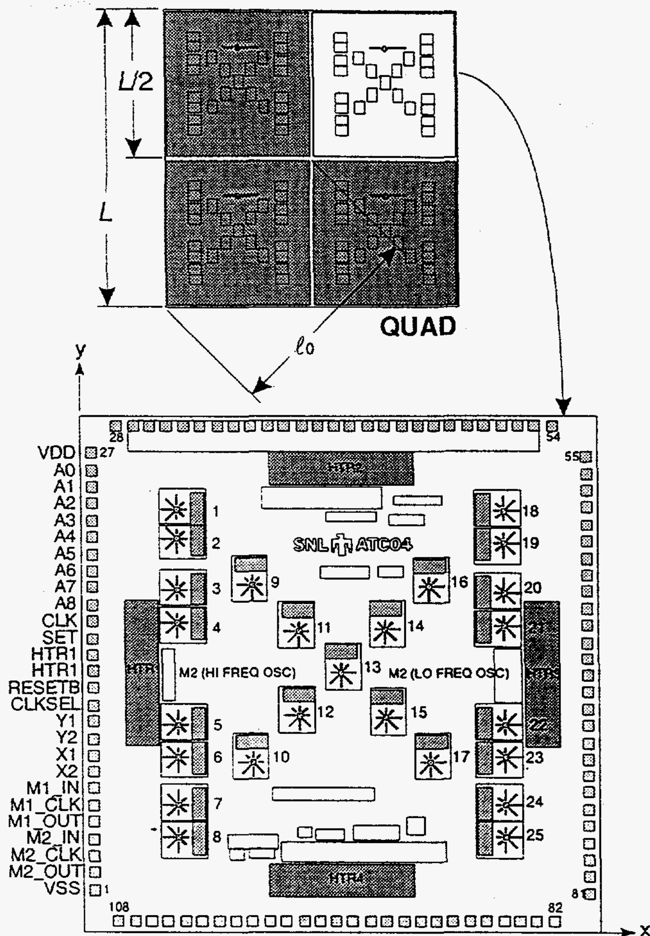


Figure1: Layout of 1 of 4 die in an ATC4 QUAD prior to redistribution and solder bumping. The first 27 perimeter bondpads are replicated around the die, so that the QUAD has perimeter access to all stress measurement circuitry. QUAD diagonal and width dimensions are shown.

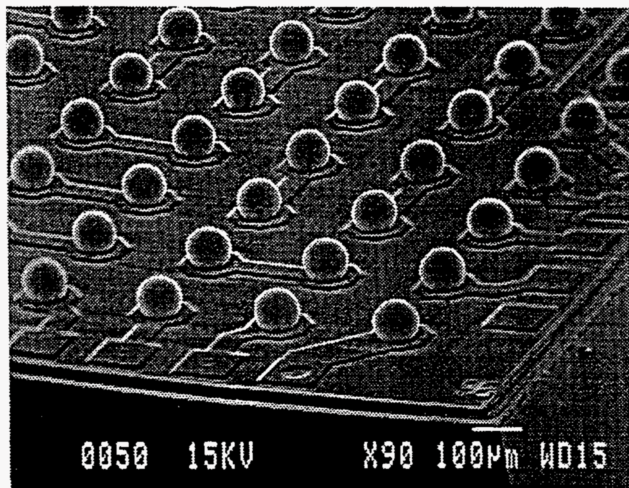


Figure 2: SEM micrograph of the corner of an ATC04.1 QUAD showing the redistributed perimeter pads and 0.0254 mm (0.010 in.) pitch solder bump array formed on the IC surface.

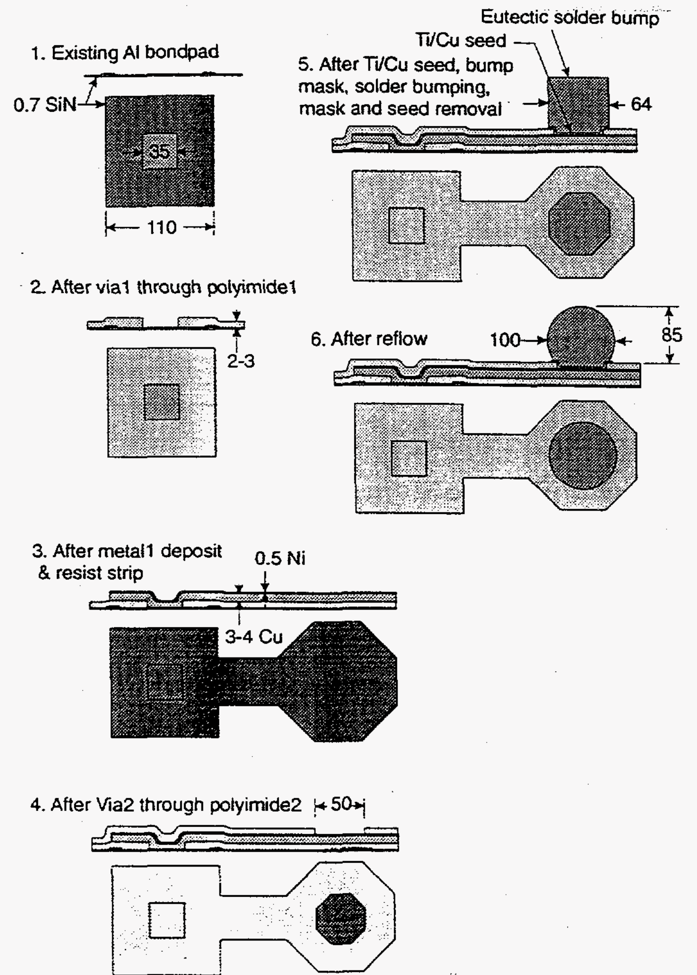


Figure 3: ATC4.1 wafer level repattern and solder bump process flow by Aptos Corporation. Dimensions are in microns.

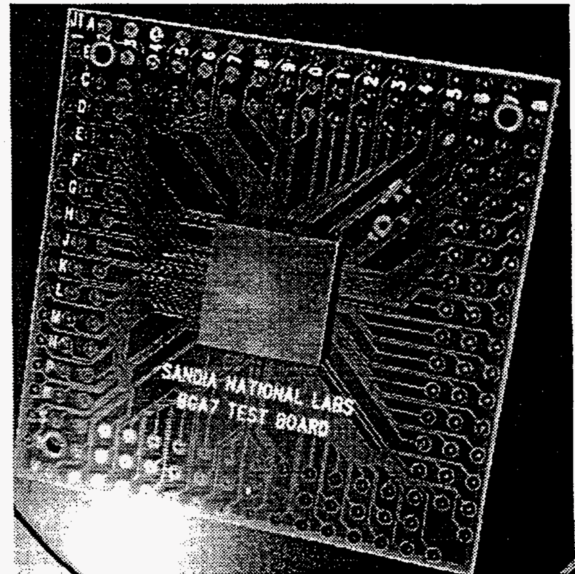


Figure 4: ATC4.1 QUAD assembled to FR-4 test board prior to underfill.

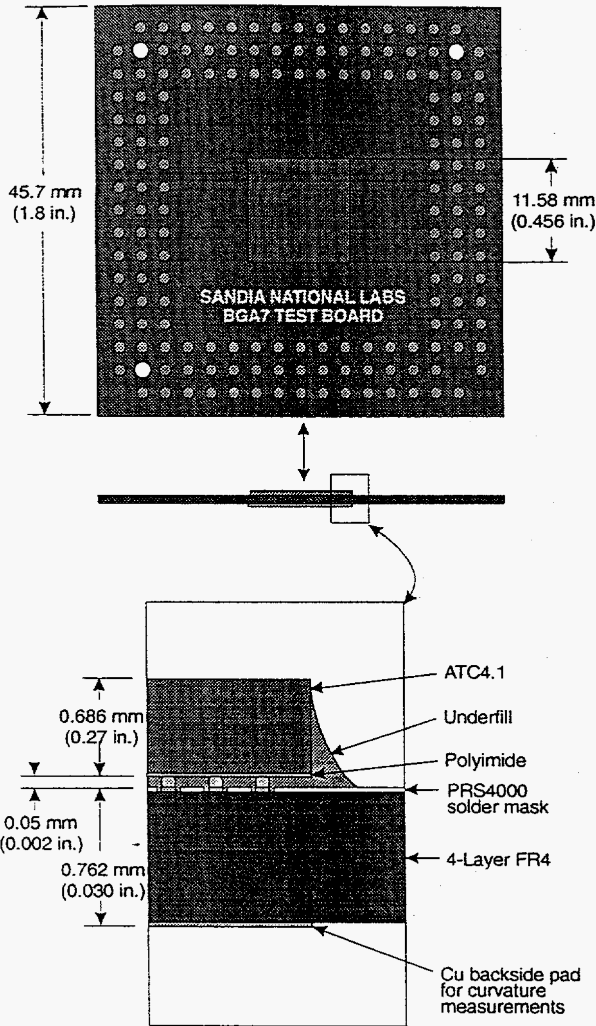


**Figure 5: Construction details of ATC4.1 QUAD flip-chip assembled on FR-4 test board.**

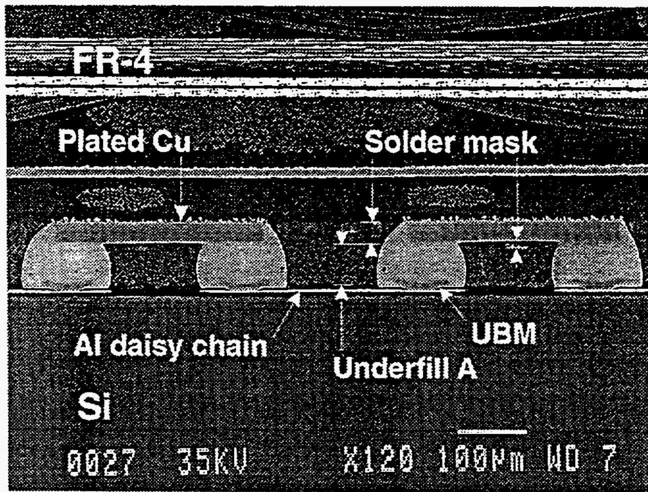


**Figure 6: SEM micrograph of ATC4.1 QUAD A11-03 cross-section.**

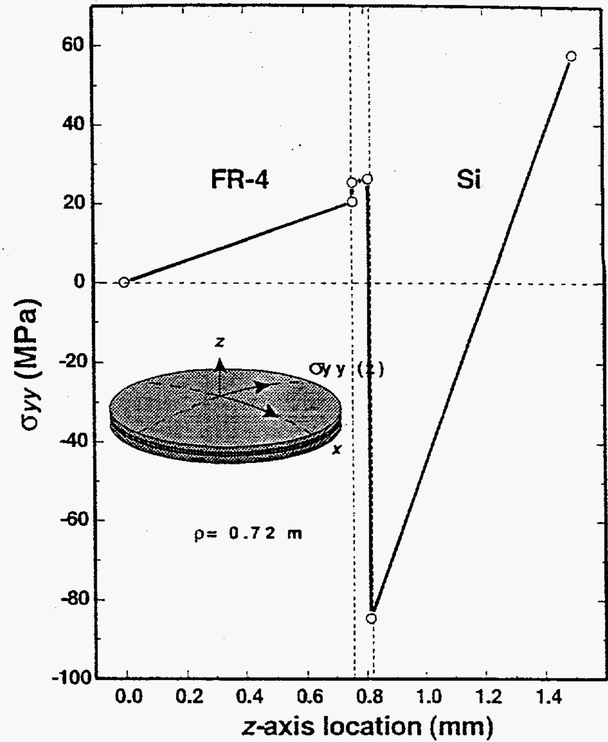


**Figure 7: In-plane stress calculated along $z$-axis and radius of curvature for infinite tri-material disk based on Hall [4]. Calculations were done for underfill A with $\Delta T$ = -140 °C.**

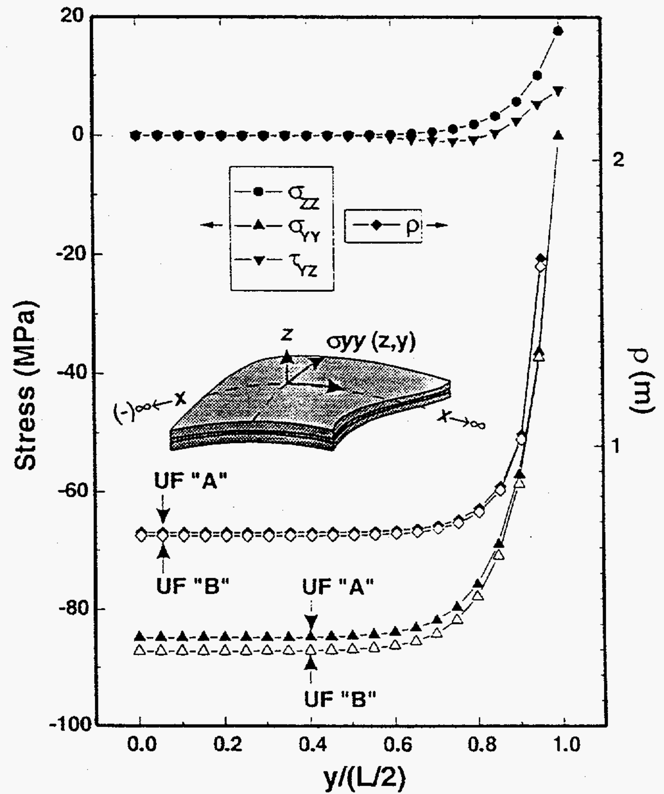


**Figure 8: Calculations based on Suhir [5,7]. Half width of QUAD is normalized. Calculations were done for underfill A and B with $\Delta T$ = -140 °C.**

Caption should say what open and filled symbols are. State what ρ is. Is Radius of curvature direction?

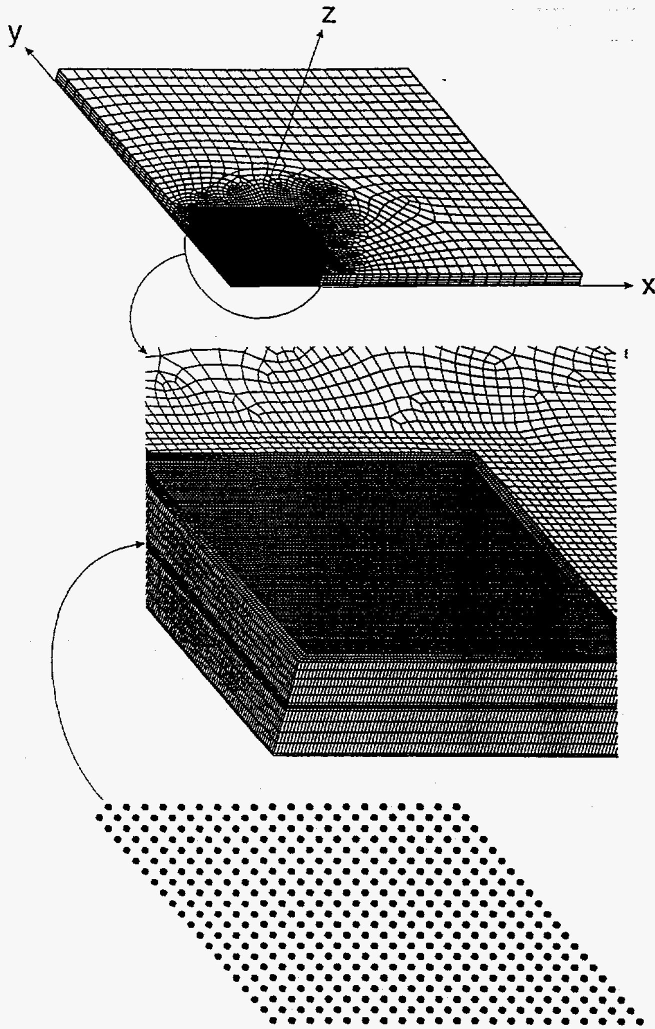


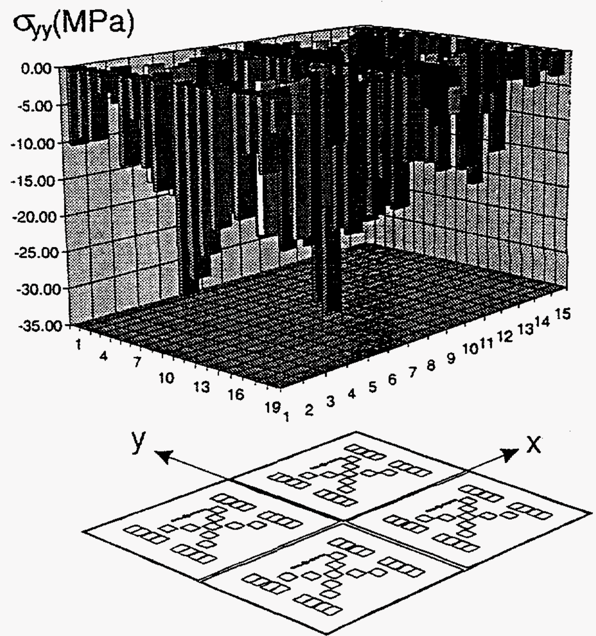


Figure 11: Measured distribution for $\sigma_{yy}$ across ATC4.1 QUAD showing decrease in stress magnitude as $y \to \pm L/2$.

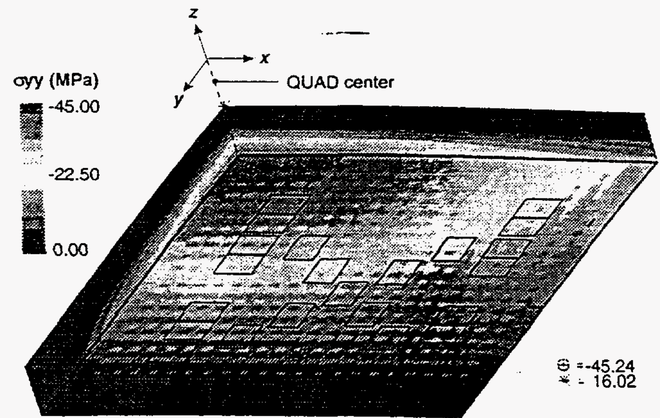


Figure 12: FEM calculated $\sigma_{yy}$ distribution in relation to stress sensor cell locations across QUAD quarter section die face prior to underfill

Figure 9: Finite element mesh of ATC4.1 test vehicle quarter section for FEM analysis. Solder ball array elements are shown in enlargement at bottom.

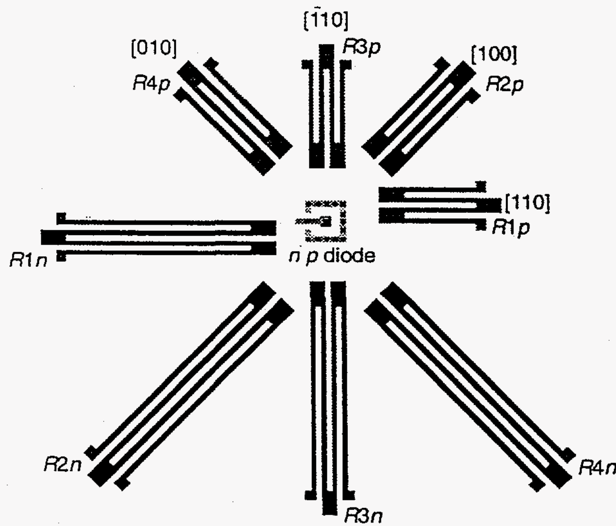


Figure 10: Stress sensor cell piezoresistor rosette showing numbering and alignment of $p$-type and $n$-type diffused resistors with crystallographic axes.

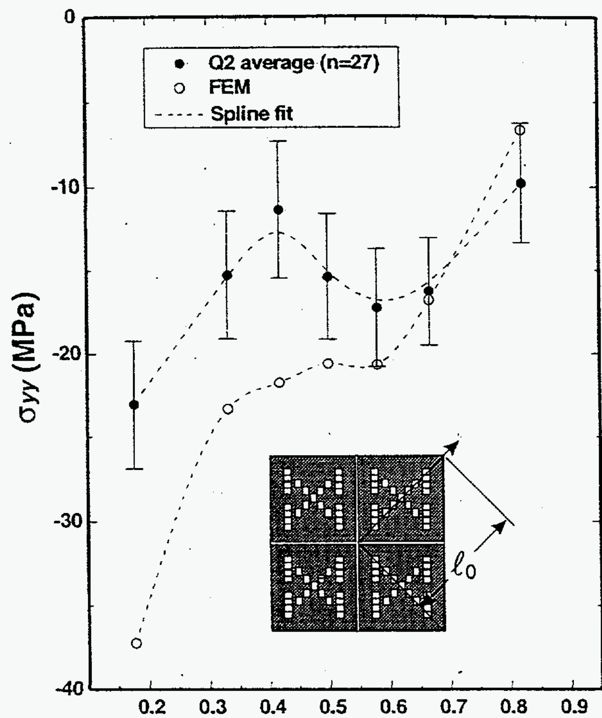


Figure 13: Average variation of $\sigma_{yy}$ (filled circles) along a chip half diagonal ($\ell_0$) prior to underfill. Error bars represent one SD. Open circles are FEM calculation for same locations. Spline fits are to aid in visualization.

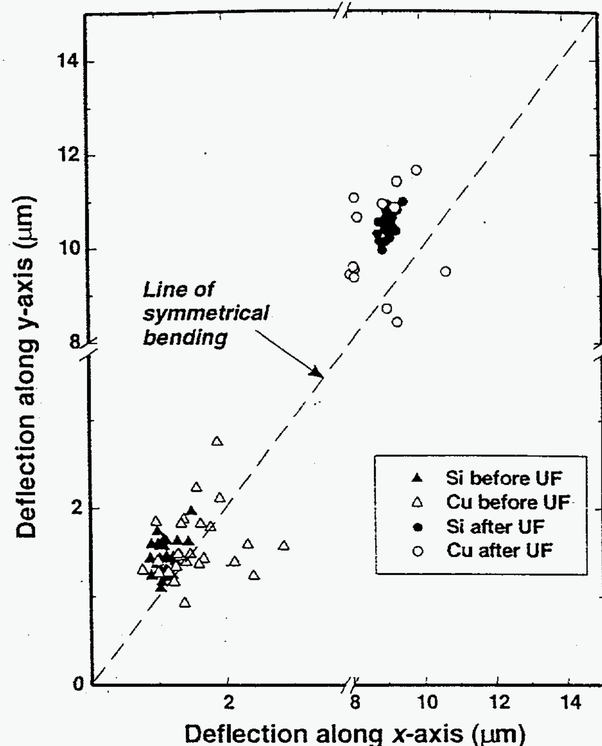


Figure 15: Plot of $y$ vs. $x$ deflection measurements of ATC4.1 QUAD backside and corresponding substrate Cu pad before (triangles) and after (circles) underfill. Symmetrical bending would result in data along the dotted line of symmetry.

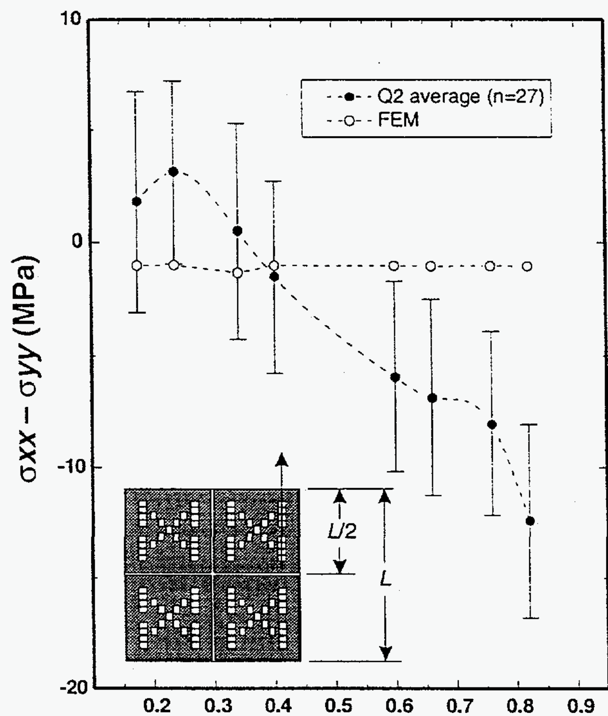


Figure 14: Average variation of $\sigma_{xx} - \sigma_{yy}$ (filled circles) along a vertical edge path as a function of distance from the center after assembly and before underfill. Error bars are one SD. Filled squares show FEM calculation for same locations.

Where are the squares?

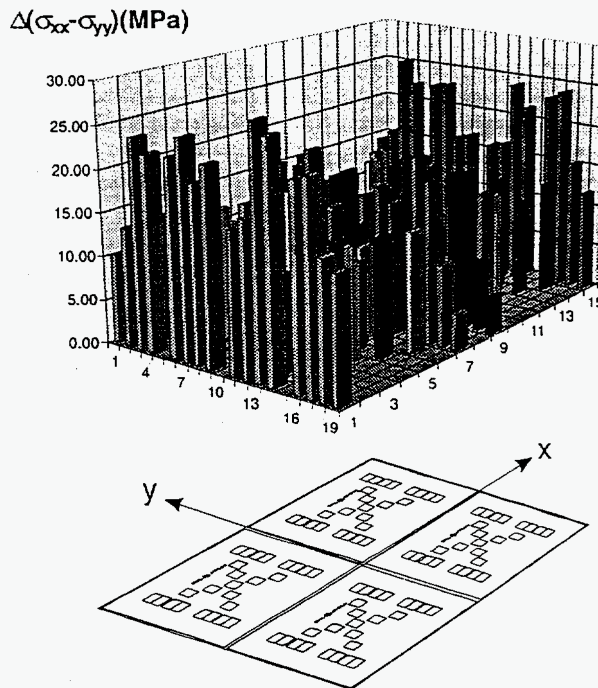


Figure 16: Change in the in-plane compressive stress difference between assembly and underfill.

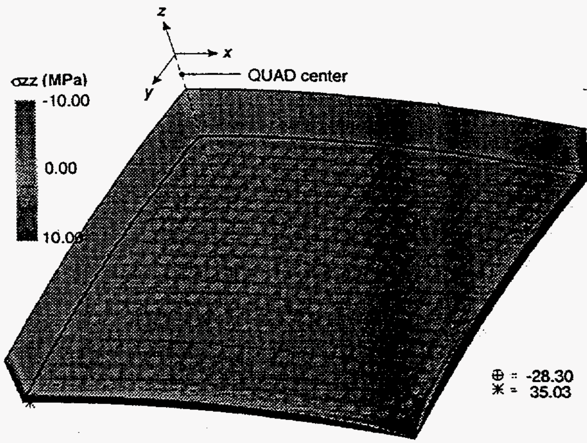


**Figure 17: FEM calculated $\sigma_{zz}$ distribution on inverted die face adjacent to underfill and substrate across QUAD quarter section based on FEM calculations after assembly using underfill A. Note stress reversal in corner.**

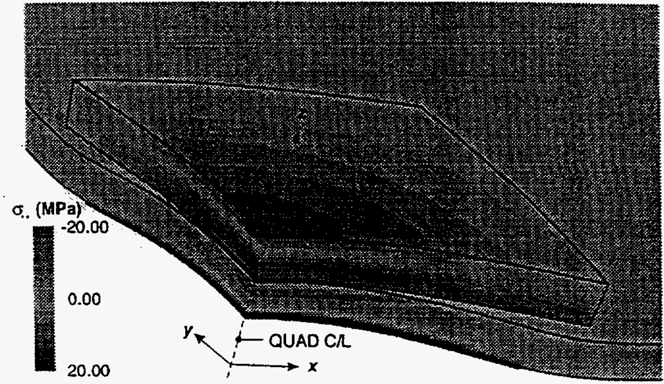


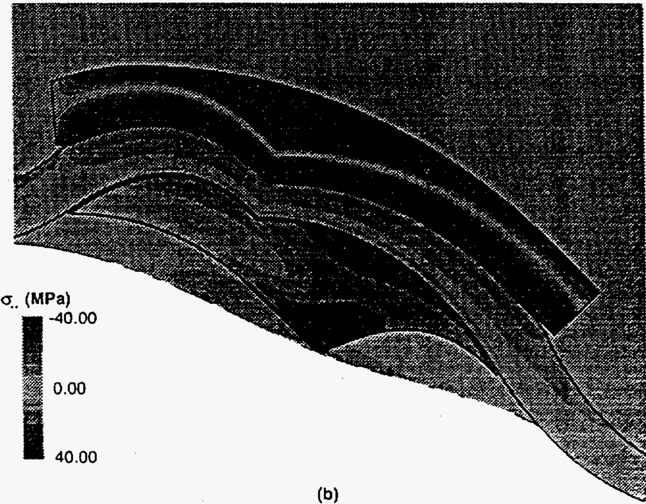


**Figure 19: $\sigma_{yy}$ FEM 3D contour plot of quarter section assembly in vicinity of die before (a) and after (b) underfill. The z-axis is magnified 400 times.**

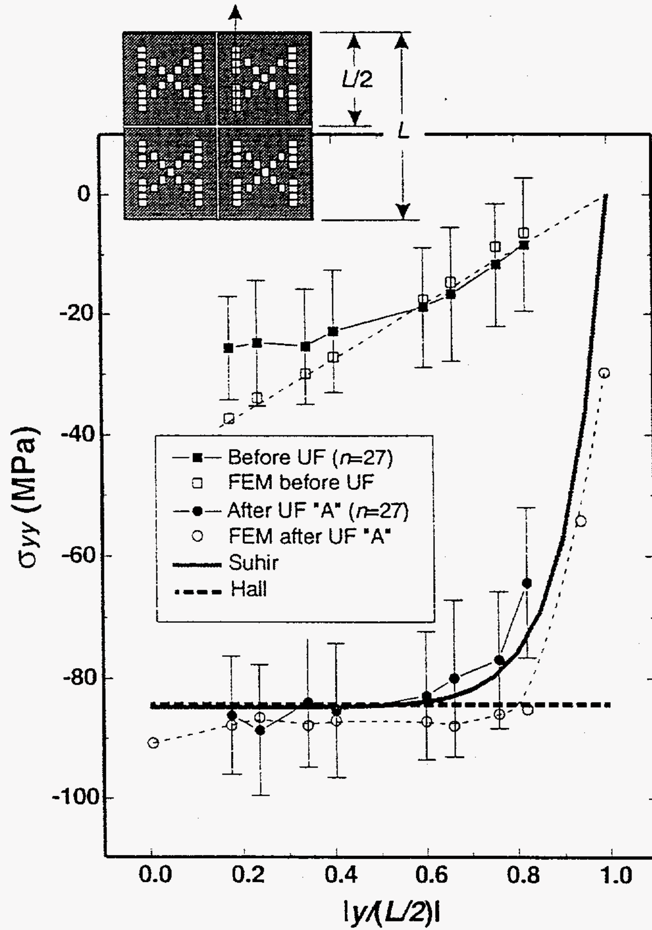


**Figure 18: Comparison of in-plane compressive stress $\sigma_{yy}$ experimental measurements to analytical and FEM calculations along centerline half length, as shown in inset. Plot contains before underfill (squares) and after underfill (circles) data and FEM calculations. Analytical calculations were done after underfill only (solid and dotted lines).**